SOILS AND FOUNDATIONS Vol. 44, No. 3, 91-101, June 2004
Japanese Geotechnical Society

ULTIMATE BEARING CAPACITY OF SOFT CLAYS REINFORCED BY A GROUP OF COLUMNS—APPLICATION TO A DEEP MIXING TECHNIQUE

M. BOUASSIDA[i] and A. PORBAHA[ii]

ABSTRACT

The ultimate bearing capacity of a soft ground, improved by end-bearing soil cement columns, is analyzed using the kinematic approach of the yield design theory. Presented here is an experimental analysis which is based on a three dimensional scaled model of the improved soft ground. The new results given by the kinematic approach and recorded experimental data are compared with others proposed by Broms' method and those established previously by the static approach of yield design theory. Regarding the results given by the Broms' method those predicted by the yield design theory approximate more accurately the recorded ultimate bearing capacity from experiments. Also, the influence of gravity forces on the bearing capacity is investigated.

Key words: bearing capacity, cohesion, group of columns, improved ground, scaled models, soft clay, soils cement columns, yield design theory (**IGC**: B12/D10/E3)

INTRODUCTION

Thickly deposited soft grounds are found abundantly in many regions around the world, particularly in the coastal areas. However, the construction of new ports and harbors on recent deposits is sometimes unavoidable to cope with economic development. In these cases, and due to the high compressibility and the lack of the bearing capacity of the ground, a soil's improvement must be done. Numerous techniques have been applied to overcome difficulties associated with the construction on soft ground. Among them, those based on granular drains (such as sand drain, and gravel drain), prefabricated vertical drains (such as cardboard drain, fabric drain, and plastic drain with jackets), vacuum consolidation, and columnar granular reinforcement (such as sand compaction piles and stone columns). Further information about these techniques has been reported in different studies (Madhav et al., 1978; Balaam et al., 1981; Bachus et al., 1985; Rixner et al., 1986; Alamgir et al., 1993; Bouassida, 1996).

For stabilization of soft grounds, in-situ deep mixing technique has been used extensively in recent years. It is a solidification technique in which the in-situ soft soil is mixed with a stabilizing material, in the form of slurry or powder, to produce stronger and firmer ground for foundations of structures. Specially designed machines with several shafts equipped with mixing blades and stabilizer injection nozzles are used to construct in-situ soil columns in various patterns and configurations (Porbaha, 1998).

In the last two decades, deep mixing technique, which has steadily progressed in Japan, Europe and the US, has been applied for solution of various problems in soft ground engineering. It has been applied, for instance, for prevention of sliding failure, reduction of settlement, excavation support, controlling seepage, preventing shear deformation and to mitigate liquefaction (Porbaha et al., 1998, 1999). Figure 1 summarizes various application areas of deep mixing. The technological aspects of deep mixing in terms of machinery and construction have progressed significantly in recent years. However, analysis and prediction of field performance for grounds improved by soil cement columns remain still empirical.

In many cases, the prediction of the bearing capacity of the reinforced soil by columns is the first verification. Previous methods have focused mainly on the isolated column model to predict bearing capacity of soils reinforced by columns. This problem has been analyzed by the use of the static approach of yield design theory (YDT) for the model of group of columns (Bouassida et al., 1995). Using the "YDT" for this model, an estimation of the bearing capacity of the reinforced soil is presented. In this study, only the kinematic approach is

[i] Dr ès Sciences, Laboratoire de Recherche《Génie civil》, Ecole Nationale d'Ingénieurs de Tunis, BP 37 Le Belvédère 1002 Tunis, Tunisia (mounir.bouassida@enit.rnu.tn).
[ii] Department of Civil Engineering, California State University, Sacramento, USA (formerly New Technology and Research-California Department of Transportation).
Manuscript was received for review on July 12, 2002.
Written discussions on this paper should be submitted before January 1, 2005 to the Japanese Geotechnical Society, 4-38-2, Sengoku, Bunkyo-ku, Tokyo 112-0011, Japan. Upon request the closing date may be extended one month.

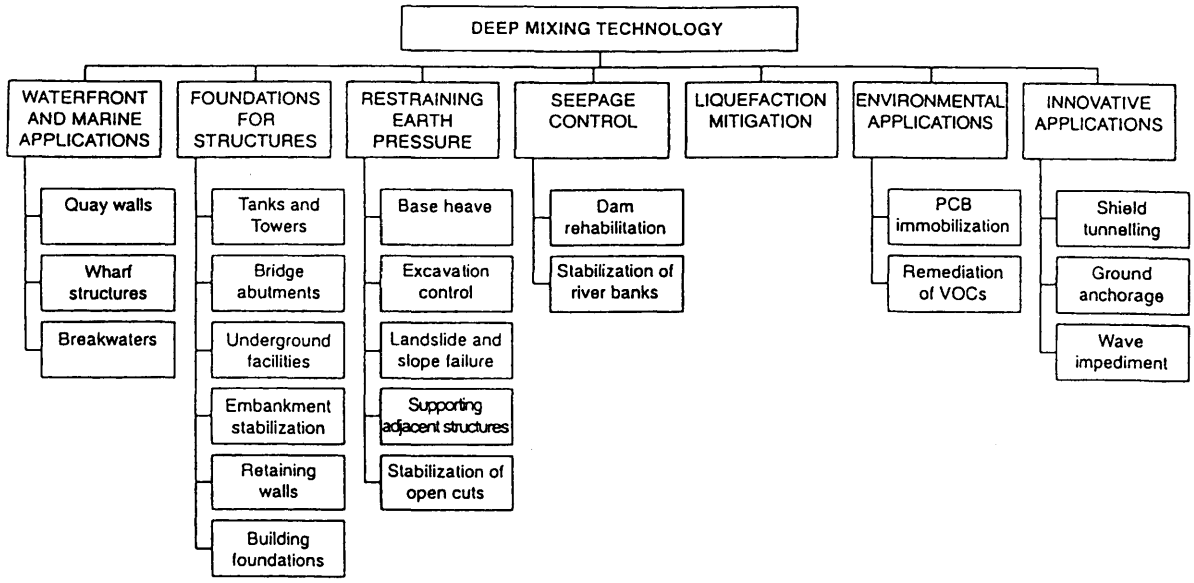

Fig. 1. Various applications of deep mixing technology, Porbaha et al. (1998)

developed for three dimensional models. While for the static approach we refer to results established by Bouassida et al. (1995).

The YDT performed here is based on fundamental concepts formulated by Salençon (1990) in the framework of continuum mechanics. Regarding the previous design methods the main advantage of YDT is its direct applicability to the group of columns modelling which still remains unusual accepting the contribution proposed by Bouassida et al. (1995). Then, the present paper aims to assess the predicted results using the group of columns modelling with experimental data recorded from loading tests conducted on three dimensional scaled models of soft clays reinforced by cemented columns. These results are compared with those issued from the Broms' method currently used in calculation reserved for deep mixing technique.

EXPERIMENTAL INVESTIGATIONS

Material Properties

The clay used in this study for the soft ground is Kaolin clay. The properties of Kaolin are as follows: liquid limit of 59, plasticity index of 42, and specific gravity of 2.692. Kawasaki clay was used for construction of soil cement columns. The properties of Kawasaki clay are as follows: liquid limit of 83, plasticity index of 45, specific gravity of 2.688. Shear strength is measured by conducting unconfined compression tests on representative specimens immediately after model tests. These tests qualified as the reliable way in determining the short term shear strength of the soft clay and they were conducted based on the JGS T 511-1990 standard reported by the JGS (1990). Obviously it was assumed that gravity force of the soft clay does not affect its shear strength which depends solely on the magnitude of the applied load during consolidation. The specimens of 35 mm in diameter and 75 mm in height were tested under controlled displacement rate of 1 mm/min. Three specimens were prepared for each case, and the specimen with best physical quality, i.e. with minimum disturbance, was tested for each case.

Toyoura sand was used for the drainage layer under the soft clay model and for the mattress at the top of the scaled models of the improved ground. The properties of Toyoura sand are as follows: mean diameter of 0.16 mm, coefficient of uniformity of 1.46, and specific gravity of 2.64. The particles are sub-angular to angular in shape with a high content of quartz. The maximum and minimum values of dry unit weight determined by the method specified by the Japanese Geotechnical Society are 16.11 and 13.09 kN/m^3, respectively (Huang et al., 1990).

Soft Ground Construction

Scaled models of the soft ground are prepared in a rigid box 500 mm by 200 mm in area and 345 mm in depth. The sides of the box are stiffened to avoid lateral movement at the time of soft soil placement and loading of the scaled models of the improved ground. The side walls of the box are sprayed with a thin layer of silicon grease to minimize end effects. One side of the box has a detachable thick rigid Plexiglas window to allow real time monitoring of the scaled models movement during loading tests.

The Kaolin clay, currently used in laboratory investigations in a remolded state, is chosen for the construction of the soft ground to ensure a better homogeneity within the scaled models. The Kaolin clay is mixed thoroughly at a water content of 120% by an electric mixer under vacuum. The homogeneous clay slurry is poured on to a 30 mm thick drainage layer of Toyoura sand at the bottom of the box. A Plexiglas plate with a large number of regular tiny drilled holes is placed at the top of the

scaled models. Drainage from the top and bottom of the clay layer is allowed during consolidation.

Consolidation of clay slurry is conducted gradually by increasing the vertical load in increments to a final stress of 30 to 50 kN/m^2 using a hydraulic cylinder which is maintained for a period of at least three days. Despite the installation of a thin silicon layer, spread in the side walls of the box, after the consolidation of the soft clay the homogeneity of the improved ground will be assumed as fulfilled, consequently the end effects are minimized. Indeed, the bearing capacity is mainly governed by the response of the ground beneath the rigid foundation by which the punching is exerted.

Columns Installation

Many factors influence the strength of soil cement including: type of soil and cement, water cement ratio, and curing time. In this series of tests, the relative strength of the columns to that of the soft soil is targeted within the ratio of 10 to 40, which is typical of the range achieved in the field (Terashi et al., 1983). Accordingly, laboratory tests were conducted on specimens, of 35 mm in diameter and 75 mm in height, of Kawasaki clay mixed with 12% ordinary Portland cement and cured for a period ranging from 7 to 14 days to achieve the target range of strength ratios. The Kawasaki clay is used to obtain more realistic characteristics of the material columns when mixed with cement and followed by the specified curing time. Therefore the expected undrained cohesion as recorded in the field will be obtained. The columns with diameter of 20 mm were made on a laboratory floor by Kawasaki clay using the same procedure carried out by Kitazume et al. (1996).

To install the columns a thin-wall aluminum tube with an outside diameter of 20 mm is pushed slowly into the soft clay at predetermined locations in a rectangular pattern (Fig. 2). The tube is aligned along a thick Plexiglas frame with predrilled holes equivalent to the targeted replacement area ratio of 18.8%. The columns were arranged in the regular rectangular pattern after removing the tube filled up by soft remolded Kawasaki clay. A mattress of 10 mm in thickness of Toyoura sand is built at the top of the improved ground, overlaid by a rigid plate as shown in Fig. 3. The scaled model of the improved ground is maintained fully saturated two days before the loading test is performed.

The Loading Tests

A rigid plate of 75 mm in width and 200 mm in length is mounted at the top of the scaled model of the improved ground, and is adjusted symmetrically to the center line of the sand mattress. Each test involves the loading of the scaled model by gradually increasing the load using a hydraulic jack until failure is observed. During the tests conducted on scaled models, the loading rate was 1 mm/min that refers to the undrained behavior of the improved soil. Such condition is representative for Kaolin clay being the soil to reinforce and columns material in terms of its strength characteristics. The loaded plate is assembled by a pin to allow rotation in the longitudinal direction of the box. Table 1 lists the geometrical configurations, physical properties, and the failure load for different scaled models of the improved ground. The vertical stress displacement curves recorded for the scaled models tested in this study are shown in Fig. 4. For the tested scaled models the failure load corresponds to the

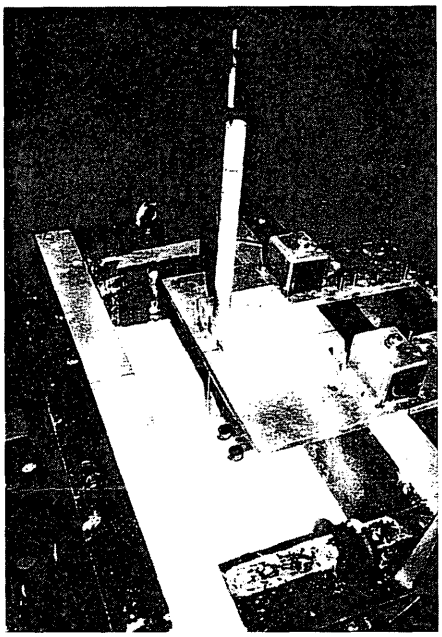

Fig. 2. Installation of soil cement columns in the scaled model

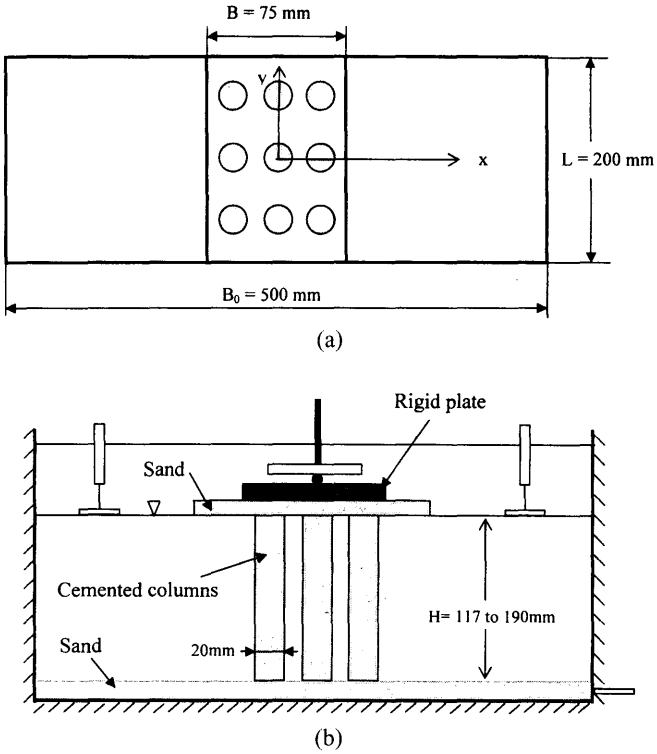

Fig. 3. Schematic diagram of a typical scaled model of the improved ground

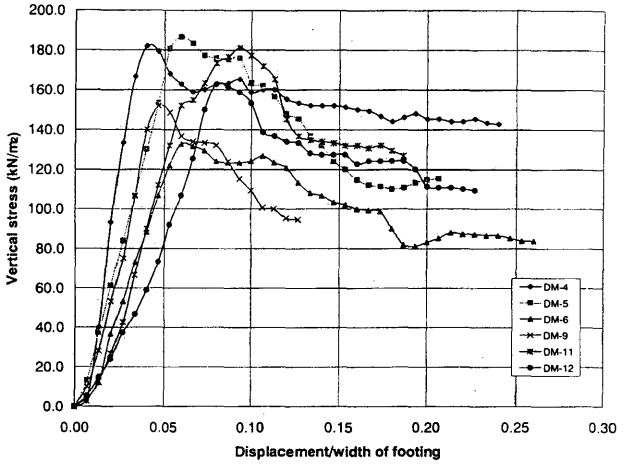

Fig. 4. Vertical stress vs displacement-width of footing curves obtained from experiments

peak of experimental curves (Fig. 4) recording the mean vertical stress (Q/BL) as a function of the normalized vertical displacement of the rigid plate. The peak load values in Fig. 4 are all recorded for normalized vertical displacements less than 10% that could be accepted reasonable in the range of small strains. The loading tests are conducted until a minimum decrease of 20% of the recorded peak load. As illustrated in Fig. 4 this condition occurred generally for a normalized vertical displacement by 20%.

ANALYSIS OF RESULTS

The theoretical framework of "YDT" has been presented by Salençon (1983, 1990). The kinematic approach of YDT is based on the construction of velocity fields being piecewise continuous and differentiable by satisfying velocity boundary conditions i.e. kinematically admissible. An upper bound of the extreme load is obtained by applying the kinematic theorem that states:

$$W_{ext}(v) \leq P(v) \tag{1}$$

where $W_{ext}(v)$ denotes the work of external forces in a given velocity field v, which is expressed as (Salençon, 1983):

$$W_{ext}(v) = \int_{\Omega} f \cdot v d\Omega + \int_{\partial\Omega} T \cdot v dS \tag{2}$$

where Ω is the domain of the scaled model of the improved ground, $\partial\Omega$ is its boundary, dS is an elementary surface, f is the volumetric forces vector and T is the stress vector. $P(v)$ in Eq. (1) is the maximum resisting work involved, in the velocity field v, which is defined as (Salençon, 1990):

$$P(v) = \int_{\Omega} \Pi(d) d\Omega + \int_{\Sigma} \Pi(n, [v]) d\Sigma \tag{3}$$

where $[v]$ is the velocity jump across the velocity discontinuity surfaces Σ in the domain Ω, and d is the strain rate tensor generated by the constructed velocity field v. In

Table 1. Geometrical and mechanical characteristics of the scaled model of the improved ground

Model No.	H (mm)	H/B	c_{us} (kN/m²)	q_{uc} (kN/m²)	K_c	Failure load (*) (kN)
DM-4	188	2.51	14.1	644	22.8	2.73
DM-5	190	2.53	15.7	584	18.6	2.80
DM-6	185	2.47	9.4	518	27.2	1.99
DM-9	188	2.51	11.0	533	25.4	2.28
DM-11	122	1.63	12.6	714	26.1	2.72
DM-12	117	1.56	9.5	695	36.6	2.44

H = thickness of the soft ground (mm), B = width of the rigid footing (mm), c_{us} = soil cohesion (kN/m²), q_{uc} = unconfined compressive strength of cement-treated columns (kN/m²), K_c = relative cohesion ratio of the column to the soft soil, Replacement area ratio is $\eta = 0.18$. (*) recorded from the peak of curves shown in Fig. 4.

Eq. (3) n is the unitary outward normal vector to any surface belonging to Σ where discontinuities of velocity occur. Starting from the expression of yield criterion $\Pi(d)$ and $\Pi(n, [v])$ are two different functions involved in the calculation of the maximum resisting energy (*see* APPENDIX I for derivation) developed when considering a given kinematically admissible velocity field (Salençon, 1990).

Hypothesis and Boundary Conditions

The materials of the scaled model (i.e., soft clay and the cement columns) are assumed to be homogeneous and isotropic continuum, their resistance is governed by Tresca's criterion (Salençon, 1983); therefore they are assumed to be purely cohesive materials. This hypothesis is well adequate and also representative, especially, for the undrained behaviour of improved soft clays when mixed by a low percentage of cement (i.e. less than 15%). Consequently, the shear resistance of such improved clays does not generate a significant angle of friction that can be generally neglected (Broms, 2000). At the contrary, their cohesion is significantly high regarding that of the unimproved state. As a matter of fact, from Table 1, the cohesion ratio of the cemented clay to that remoulded in the laboratory is given by: $18 < K_c < 37$.

For the formulation of this system all variables are expressed in the local basis with unitary vectors e_x, e_y and e_z.

By assuming compressive stresses to be negative, the convention commonly used in continuum mechanics (Salençon, 1990), boundary conditions of the scaled model of the improved ground are as follows (Fig. 5(a)):

(a) At the surface of the scaled model ($z = 0$):

$$\forall (x, y) \in S \quad v = -Ue_z \quad (U > 0) \tag{4}$$

$$\forall (x, y) \notin S \quad T = 0 \tag{5}$$

where U is the vertical component of the vector of velocity displacement applied by the rigid footing with cross section $S = BL$.

(b) At the bottom of the scaled model: ($z = -H$ and $\forall (x, y)$) velocity displacement is null

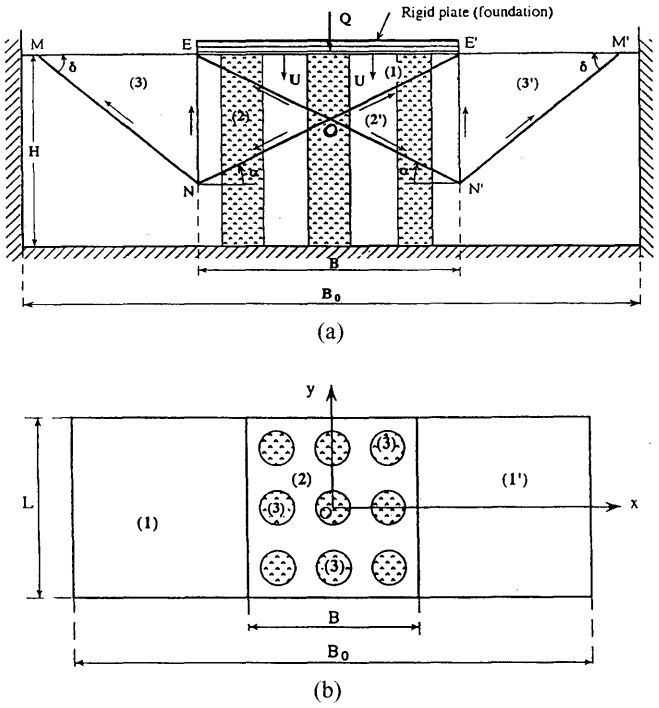

Fig. 5. The failure mechanism with five blocks (a) cross section and (b) plane view

$$v_x = v_y = v_z = 0 \tag{6}$$

(c) At the borders of the rigid box $[-H \le z \le 0]$:

$$^*x = \pm\frac{B_0}{2}: \quad T = T_x e_x; \quad v_x = 0 \tag{7a}$$

$$^*y = \pm\frac{L}{2}: \quad T = T_y e_y; \quad v_y = 0 \tag{7b}$$

where B_0 and L denote the length and the width of the rigid box, respectively.

The work of external forces is calculated from Eq. (2) by taking into account the boundary conditions given by Eqs. (4), (5), (6), (7(a) and (b)); by setting $f = -\gamma_c e_z$ for the soil cement columns, and $f = -\gamma_s e_z$ for the soft soil. This calculation leads to:

$$W_{ext}(v) = QU - \int_{\Omega_s} \gamma_s v_z d\Omega - \int_{\Omega_c} \gamma_c v_z d\Omega \tag{8}$$

where γ_s and γ_c are the unit weights of the soft soil and the column material, and Ω_s and Ω_c are the volume of the soft soil and the columns, respectively.

The vertical force Q in Eq. (8) is the loading parameter that characterises the bearing capacity of the rigid footing, which is expressed as:

$$Q = -\int_{S(z=0)} T_z dS \tag{9a}$$

The bearing capacity of the rigid footing is expressed in this paper by the dimensionless ratio that characterises the bearing capacity factor (BCF), as follows:

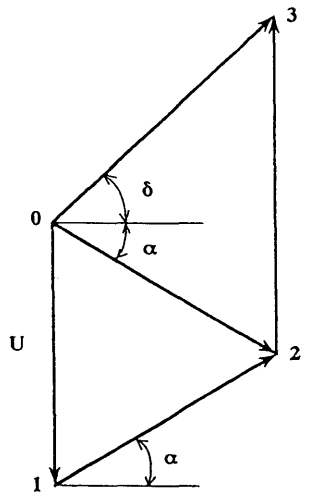

Fig. 6. The hodograph construction

$$\mathrm{BCF} = \left(\frac{Q}{c_{us} S}\right) \tag{9b}$$

in which c_{us} is cohesion of the soft clay, and S is the area of the footing. The cohesion of the material columns is equal to $K_c c_{us}$, where K_c is the cohesion ratio of the column to the soft soil ($K_c > 1$).

Two main facts govern the three dimensional aspect of the constructed scaled models. The first one is relevant from the geometry of a group of columns with cylindrical cross section. The second fact concerns the contribution of the soft soil resistance generated at the borders $y = \pm L/2$ of the models (Fig. 3). In fact, such end effects are not taken into account when dealing with plane strain studies, i.e. the case of strip footing.

Calculation of the Ultimate Bearing Capacity

A mechanism with five blocks (Fig. 5(a)) is investigated in this study. Using the hodograph construction shown in Fig. 6 the discontinuities of velocity induced on surfaces (OE), (ON), (NE), (NM) and their symmetric parts are calculated (details are given in APPENDIX I).

The mechanism with five blocks is kinematically admissible under the following conditions on the parametric angles α and δ:

$$0 < \alpha \le \arctan\left(\frac{H}{B}\right) \tag{10}$$

$$\arctan\left(\frac{2\tan\alpha}{(B_0/B)-1}\right) < \delta \le \frac{\pi}{2} \tag{11}$$

Derivation of the maximum resisting work given by Eq. (3) is compiled in APPENDIX I that yields:

$$P(\underline{v}) = c_{us} US\left\{\frac{1+\eta(K_c-1)}{\sin\alpha\cos\alpha} + \frac{1}{\sin\delta\cos\delta} + \tan\alpha + \tan\delta\right\} + kc_{us}B^2U\left(\frac{1+\sin\alpha}{2\cos\alpha} + \frac{\tan\alpha}{\sin\delta}\right) \tag{12}$$

where k is the ratio relating the soil cohesion, c_{us}, to that of the contact surface between the scaled model of the im-

proved ground and the borders of the rigid box, c'_{us}, such that at $y = \pm L/2$ (Fig. 3):

$$c'_{us} = k c_{us} \tag{13}$$

where $0 \le k < 1$.

The contribution of gravity forces appearing in Eq. (8) leads to the following expression (*see* APPENDIX II for derivation):

$$\int_{\Omega_c} \gamma_c v_z d\Omega + \int_{\Omega_s} \gamma_s v_z d\Omega = \eta(\gamma_c - \gamma_s) \frac{SBU \tan \alpha}{2} \tag{14}$$

The BCF is determined from Ineq. (1) by applying Eqs. (2), (12) and (14), that leads to:

$$\left(\frac{Q^*}{c_{us}S}\right) \le \frac{1+\eta(K_c-1)}{\sin\alpha\cos\alpha} + \tan\alpha + \frac{1}{\sin\delta\cos\delta} + \tan\delta + k\left(\frac{B}{L}\right)\left(\frac{1+\sin\alpha}{2\cos\alpha} + \frac{\tan\alpha}{\sin\delta}\right) - \eta(\gamma_c - \gamma_s)\frac{B\tan\alpha}{2c_{us}} \tag{15}$$

where Q^* denotes the theoretical extreme vertical load at failure of the reinforced ground.

The upper bound values of BCF based on the kinematic approach are determined after numerical minimization of the right side of Ineq. (15) with respect to α and δ, and taking into account the conditions stated in Eqs. (10) and (11). To achieve this task, a minimization program is implemented in which the range of α and δ ensuring the best upper bounds of BCF are as follows: $40° \le \alpha \le 43°$ and $35.2° \le \delta \le 38.6°$. Obviously these values of angles α and δ depend on values of all parameters intervening in the right hand of Ineq. (15), i.e. η, K_c, k, B/L and $(\gamma_c - \gamma_s)B/c_{us}$.

Bounding of the Ultimate Bearing Capacity

After the results presented by Bouassida et al. (1995, 1998), in the case of soft clays reinforced by end-bearing columns both assumed as purely cohesive media and having equal unit weights ($\gamma = \gamma_c = \gamma_s$) the bearing capacity factor writes:

$$\frac{Q^*}{c_{us}S} \ge 4 + 2\eta[K_c - 1] \tag{16}$$

In APPENDIX III making use of the approach by inside (called also the static approach) of YDT the lower bound given in Ineq. (16) is briefly recalled. Assuming equal unit weights ($\gamma_c = \gamma_s$) and smooth contact on borders of the scaled model of the improved ground ($k = 0$), from Ineq. (15) the derivation of the upper bound of bearing capacity is done analytically. The minimisation of the right side of Ineq. (15) is easily done analytically that leads to the best upper bound solution for angles α and δ given by:

$$\tan\alpha = \sqrt{\frac{1+\eta(K_c-1)}{2+\eta(K_c-1)}} \tag{17a}$$

$$\tan\delta = \frac{\sqrt{2}}{2}; \quad (\delta = 35.3°) \tag{17b}$$

Based on values of (H/B) presented in Table 1, the condition (10) is always satisfied for angle α calculated from Eq. (17a). Also, for angle δ defined by (17b) the condition (11) is always satisfied. Then, substituting (17a and b) in (15), and taking into account (16), the bearing capacity factor is bounded as follows:

$$4 + 2\eta[K_c - 1] \le \frac{Q^*}{c_{us}S} \le 2\sqrt{2} + 2\sqrt{[1+\eta(K_c-1)][2+\eta(K_c-1)]} \tag{18}$$

The analytical bounding of BCF given by (18) has the advantage to be employed for the case of reinforcement by a group of columns for any pattern, which is more useful in practice than the isolated column model. Nevertheless, this result is only valid in the case of a centered vertical load exerted by a rigid foundation that is the situation of the tested scaled models. In other cases such as eccentric and (or) inclined load the BCF obviously depends on the above mentioned parameters.

Furthermore, it appeared that the importance of parameters such as the improvement ratio area η and the cohesion factor K_c allows the computation of an upper bound and a lower bound of the BCF of a rigid foundation with a given cross area S resting on an improved soft ground by soil cement columns.

Predicting BCF from Broms' Method

Based on the approach proposed by Broms (2000) the ultimate bearing capacity of a ground improved by a group of end bearing columns is the sum of two independent terms, q_1 and q_2, as follows:

(a) The first term, denoted q_1, corresponds to the creep resistance of columns, it writes:

$$q_1 = \frac{n_c Q_f}{BL} \tag{19}$$

where n_c is the total number of columns located under the footing with dimensions B and L; Q_f is the creep load estimated by 70% of the unconfined compressive strength of the columns material.

(b) The second term, denoted q_2, is related to the bearing capacity of the soft soil where local shear failure is assumed, i.e.:

$$q_2 = \lambda c_{us}\left(1 + 0.2\frac{B}{L}\right) \tag{20}$$

where λ is a dimensionless coefficient for which the value $\lambda = 5.5$ was proposed (Bergado et al., 1994). This term is the bearing capacity of the unimproved ground. Using the data $B = 75$ mm, $L = 200$ mm, it comes: $(Q/c_u S)_{\text{unimproved}} = 5.9125$.

The creep load is then determined from Eq. (19) where the compressive strength of the columns is equivalent "$2K_c c_{us}$" (Bouassida et al., 1998):

$$Q_f = 1.4\eta B L K_c c_{us} \tag{21}$$

From Eqs. (19) and (21), we have:

$$\frac{q_1}{c_{us}} = 1.4\eta K_c \tag{22}$$

Table 2. Comparison of experimental results with kinematic approach calculations

Model No.	K_c	BCF_{exp}	BCF_{kin} (k=0)	BCF_{kin} (k=0.5)	BCF_{kin} (k=1.0)
DM-4	22.8	12.9	13.63	14.09	14.54
DM-5	18.6	11.9	12.11	12.57	13.00
DM-6	27.2	14.1	15.22	15.69	16.14
DM-9	25.4	13.8	14.57	15.04	15.48
DM-11	26.1	14.4	14.82	15.29	15.74
DM-12	36.6	17.1	18.61	19.09	19.54

$(BCF)_{exp}$ = bearing capacity factor obtained from the experiment, $(BCF)_{kin}$ = bearing capacity factor calculated numerically by the kinematic approach. Calculations have been done with values $\gamma_c = 17.8$ kN/m^3 and $\gamma_s = 17.2$ kN/m^3.

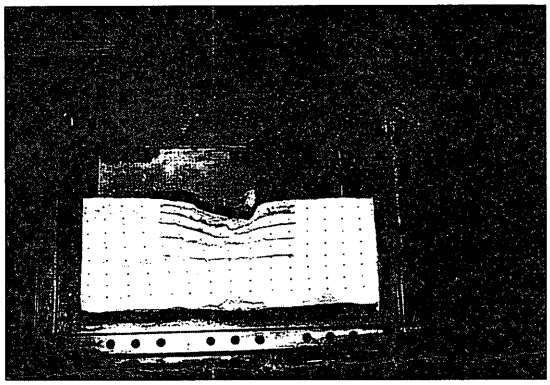

Fig. 7. Deformation pattern at failure of the scaled model DM-5

The data for the scaled model are as follows: $\eta = 0.18$ then $q_1/c_{us} = 0.252K_c$; $B/L = 0.375$; $q_2/c_{us} = 5.912$. Therefore, the estimation of BCF of the improved ground by the Broms method writes:

$$BCF = 0.252K_c + 5.912 \quad (23)$$

DISCUSSIONS OF RESULTS

Table 2 summarises the bearing capacity factors obtained from tests, carried on the scaled models of the improved ground, along with those determined numerically by the kinematic approach of YDT. For each scaled model, the experimental BCF value is calculated from the peak load Q_{peak} using Eq. (9b).

From typical "vertical stress-normalised displacement" curves (Fig. 4), the peak load of each scaled model, is determined for a ratio "vertical normalised displacement/width of footing" less than 10%, i.e., corresponding to a small deformation rate. For all tested scaled models of the improved ground, the peak load occurs in this range of the normalised-displacement. While the deformation pattern shown in Fig. 7 corresponds to the end of the loading test carried on the scaled model DM-5. At this stage, it is clear that a high deformation rate is generated in the scaled model. Indeed, the corresponding ratio "displacement/width of footing" is roughly 15% (Fig. 4).

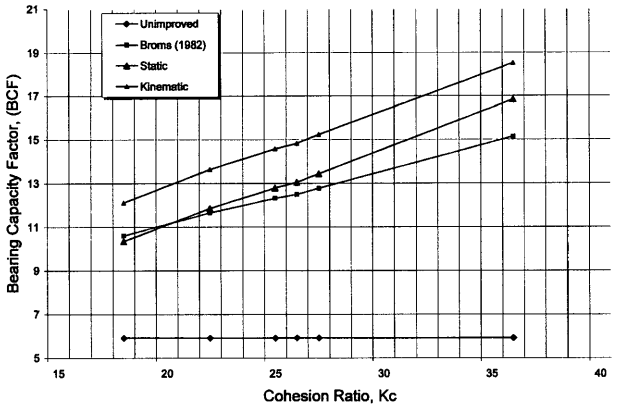

Fig. 8. BCF variation vs K_c ratio ($k = 0$; $\gamma_c = \gamma_s$)

The calculated upper bound BCF's depends on the value of k defined in Eq. (13). Indeed, from Table 2 the absolute values of relative differences between the experimental results and those of BCF determined numerically from the kinematic approach are within 2% to 9% for the assumption of smooth contact ($k = 0$), and within 5.6% to 11.6% in the case of medium roughness ($k = 0.5$). In the absence of an experimental method to determine k, the choice of $k = 0.5$ could be considered in the calculations. Although, compared to the case where $k = 0$, Table 2 illustrates no significant dependence of the BCF values on k, i.e., between 2.6% and 3.8%.

The maximum relative difference between upper bound of BCF and that recorded from experiments occurs for DM-12, i.e. the scaled model with the highest cohesion ratio ($K_c = 36.6$). Indeed, from the upper bound expression given in Ineq. (15) if the cohesion ratio increases the upper bound of BCF is too. The recorded values of BCF from scaled models confirm also this finding. From Fig. 8 one can observe when K_c increases theoretical upper bound values are a little bit more pronounced than those recorded from the experiments. As a matter of fact, using a linear regression estimate for the two methods it comes ($18 \le K_c \le 37$):

$$\left(\frac{Q}{c_u S}\right)_{kin} = 0.3611K_c + 5.397$$

$$\left(\frac{Q}{c_u S}\right)_{exp} = 0.2914K_c + 6.3905$$

Although the mechanism of five blocks seems simple, prediction of BCF by this failure model is acceptable in practical use. Indeed, in the case of equal unit weights $\gamma_c = \gamma_s$, $k = 0$, the upper bound solution given by this mechanism is analytical, and it is valid for any column pattern. The relative differences between upper bounds, derived by the five blocks mechanism, and recorded BCF values from tests range from 1.8% to 8.8% (Table 3). Nevertheless, the construction of more elaborated velocity fields—such as those inducing deformation within the improved ground would lead to better upper bounds of the BCF, i.e. lower than the upper bound obtained by the

Table 3. Comparison of experimental results with yield design theory approaches

Model specimens	Cohesion ratio (K_c)	$(BCF)_{stat}$ (a)	$(BCF)_{kin}$ (b)	$(BCF)_{exp}$ (c)	Relative difference (%) (c) to (a)	Relative difference (%) (b) to (c)
DM-4	22.8	11.85	13.63	12.9	8.7	5.7
DM-5	18.6	10.34	12.11	11.9	5.1	1.8
DM-6	27.2	13.43	15.22	14.1	5.0	7.9
DM-9	25.4	12.78	14.57	13.8	8.0	5.6
DM-11	26.1	13.04	14.82	14.4	10.4	2.9
DM-12	36.6	16.82	18.61	17.1	1.8	8.8

$k=0$, $\gamma_c=\gamma_s$, $(BCF)_{stat}$ = bearing capacity factor calculated by the static approach, $(BCF)_{exp}$ = bearing capacity factor obtained from the experiment, $(BCF)_{kin}$ = bearing capacity factor calculated analytically by the kinematic approach.

Table 4. Comparison of experimental results with Broms' method

Model No.	K_c	$(BCF)_{exp}$	$(BCF)_{Brm}$	Relative difference (%)
DM-4	22.8	12.9	11.65	10.7
DM-5	18.6	11.9	10.60	12.3
DM-6	27.2	14.1	12.77	10.4
DM-9	25.4	13.8	12.31	12.1
DM-11	26.1	14.4	12.49	15.3
DM-12	36.6	17.1	15.13	13.0

$k=0$, $(BCF)_{exp}$ = bearing capacity factor obtained from the experiment, $(BCF)_{Brm}$ = bearing capacity factor estimated from Broms' method.

mechanism of five blocks considered in this study.

Comparison between failure mechanisms: Comparing between the five blocks mechanism failure and the experimental one, it should be noted that the theoretical determination of the upper bound of BCF remains valid for any kinematically admissible velocity field (considerations of the principle of virtual work, Salençon, 1990). Consequently, the similarity between observed and "imagined" mechanisms is not necessary. Although symmetric mechanisms are preferred due to the geometrical and mechanical symmetry of the model. While in the observed mechanism, failure during tests is related to many experimental conditions such as: homogeneity of the reconstituted clay, columns installation, the loading system, etc.

It should be also noted that upper bound values of BCF derived numerically (Table 2) and analytically (Table 3) are identical in the case $\gamma_c=\gamma_s$, $k=0$. This result shows that the implemented program for upper bound calculation is reliable.

Furthermore, in the case $k=0$ (smooth contact between the soft ground and the caisson borders), comparing between $(BCF)_{kin}$ values presented in Tables 2 and 3, the influence of gravity remains insignificant when predicting the upper bound of BCF in the reinforcement case of purely cohesive materials.

Despite limitations with experimental work, i.e., the scale effect, end effects, stress gradient, and so alike, that may have contributed to the discrepancies, the overall estimations appear to be satisfactory. All the experimental data relevant to the BCF's are lower than the predicted values that serve as the least upper bound solution, and they are greater than those given by the lower bound solution (Fig. 8). In addition, from practical viewpoint, the relative differences between the experimental and the theoretical calculations of BCF are not considerable.

For the tested scaled models, with replacement area ratio $\eta=0.18$, results presented in Table 4 summarise lower and upper bounds values of BCF derived from (16) and (18), and those determined by Broms' method and recorded values from the experiments. The estimation of BCF for all scaled models, using Broms' method, in which the relative difference with the experimental results is 10% to 14%.

From Fig. 8 it appears that prediction of BCF becomes more underestimated by Broms' method when the cohesion ratio K_c increases. Hence, that applicability of Broms' method could be restricted to the range of K_c values less than 30.

Regarding the Broms' method, the kinematic approach of YDT which developed here is more realistic, especially because of the group of columns modelling which is elaborated in a well established framework which is an original aspect. Also, the YDT approaches are applicable for any columns reinforcement technique. This result, illustrated in Fig. 8 shows the efficiency of YDT approaches investigated here.

As a conclusion, it should be noted that the recorded values of BCF from experiments are well bounded by the analytical solutions in acceptable margin of error for soil mechanics use (i.e. less than 10.4%). This result is illustrated in Table 3 through relative differences "(c) to (a)" and "(b) to (c)".

CONCLUSIONS

Based on yield design theory, a method of analysis has been presented to determine the bearing capacity of a model footing resting on a soft cohesive ground improved by a group of soil cement columns. Scaled three-dimensional models have been constructed using remoulded soft clay improved by soil cement columns and tested until failure. The main findings of this work are the following:

1) Through experimental investigations, it was shown that both the kinematic and the static solutions of yield design theory could be a promising tool to determine an acceptable bounding of the bearing capacity of soft ground improved by soil cement group of columns. For a better validation of this result, comparison was made with the approach proposed by Broms (2000) in which the relative differences were found to be in the range of 10% to 14%. Nevertheless, regarding to experimental results, estimation of the bearing capacity by Broms' method tends to be underestimated if the cohesion ratio becomes greater than 30.

2) With respect to previous contributions, the main advantage of the proposed design method remains in the use of the improvement area ratio as a principal

parameter for computing the bearing capacity factor of soft grounds improved by soil cement columns.

3) This study should be regarded as a preliminary step in the analysis of cement columns improved ground. Further tests and ideally pilot field studies should be carried out to shed light on the applicability of the technique under various loading conditions with different reinforcing configurations of the columns and values of the improvement area ratio.

NOTATION

b: distance (m)
B: width of the footing (m)
B_0: Length of the scaled model of the improved ground (m)
c_{us}: soil cohesion (kN/m^2)
c'_{us}: cohesion of contact surface between clay and sides of the rigid box (kN/m^2)
c_{us}: cohesion of soft soil (kN/m^2)
d: strain rate tensor
e_x, e_y, e_z: unit vectors
f: vector of volumetric forces (kN/m^3)
H: thickness of the scaled model of the improved ground (m)
K_c: cohesion ratio of the column to the soft soil
k: cohesion ratio of the rigid box sides interfacing the soft soil
L: length of the footing (m)
n: outward unit normal vector
n_c: number of columns
S: area of the footing ($S=BL$), (m^2)
$P(v)$: maximum resisting work (kN·m/s)
$q_{1,2}$: uniform vertical stress (kN/m^2)
q_{uc}: :unconfined compressive strength of cement-treated columns (kN/m^2)
Q: compressive force exerted by the footing (kN)
Q_{peak}: measured peak load (kN)
T: stress vector (kN/m^2)
U: compressive vertical velocity displacement (m/s)
x_i: components of the position vector of a point M (m)
x, y, z: variables expressed in the e_x, e_y, e_z space
V: volume (m^3)
v: velocity field vector (m/s)
$[v]$: discontinuity of velocity across the surfaces Σ in the domain Ω (m/s)
$W_{ext}(v)$: the work of external forces in a given velocity field (kN·m/s)
α, δ: angles (degrees)
γ_c: unit weight of column material (kN/m^3)
γ_s: unit weight of soil (kN/m^3)
λ: coefficient used in Broms' method
Ω_c: domain of the scaled model of the improved ground occupied by the columns (m^3)
Ω_s: domain of the scaled model of the improved ground occupied by the soft soil (m^3)
Σ: set of surfaces where discontinuities of velocity occur
η: replacement area ratio
Ω: domain of the scaled model of the improved ground
$\partial\Omega$: boundary of the scaled model of the improved ground
Π: positive function characterising the maximum dissipated energy per unit volume

Subscripts:
c(s): column (soil)

REFERENCES

1) Alamgir, M., Miura, N. and Madhav, M. R. (1993): Analysis of granular column reinforced ground, *Report of Faculty of Science and Engineering*, Saga University, Japan, **22**(1), 66, 111-118.
2) Bachus, R. C. and Barksdale, R. D. (1985): Vertical and lateral behavior of model stone columns, *Int. Conf. on In-Situ Soil and Rock Reinforcement*, Paris, 99-104.
3) Balaam, N. P. and Booker, J. R. (1981): Analysis of rigid rafts supported by granular piles, *International Journal for Numerical and Analytical Methods in Geomechanics*, **5**, 379-403.
4) Bergado, D. T., Chai, J. C., Alfaro, M. C. and Balasubramaniam, A. S. (1994): Improvement techniques of soft ground in subsiding and lowland environment, Balkema, Rotterdam, The Netherlands, 1-220.
5) Bouassida, M. (1996): Etude expérimentale du renforcement de la vase de Tunis par colonnes de sable—Application pour la validation de la résistance en compression théorique d'une cellule composite confinée, *Revue Française de Géotechnique*, **75**, 3-12.
6) Bouassida, M., de Buhan, P. and Dormieux, L. (1995): Bearing capacity of a foundation resting on a soil reinforced by a group of columns, *Géotechnique*, **45**(1), 25-34.
7) Bouassida, M. and Hadhri, T. (1998): Capacité portante d'une fondation posée sur un sol renforcé par colonnes, *Revue Marocaine de Génie Civil.*, **78**, 2-16.
8) Broms, B. G. (2000): Lime and lime/columns. Summary and visions. *Proc. 4th Int. Conf. on Ground Improvement Geosystems, Keynotes Lecture*, Helsinki, June 7-9, 43-93.
9) Huang, C. and Tatsuoka, F. (1990): Bearing capacity of reinforced horizontal sandy ground, *Geotextiles and Geomembranes*, **9**, 51-82.
10) Japanese Geotechnical Society (1990): Manual of soil testing and methods, JGS T 511-1990, Japanese Geotechnical Society, Tokyo, 320 (in Japanese).
11) Kitazume, M., Ikeda, T., Miyajima, S. and Karastanev, D. (1996): Bearing capacity of improved ground with columns type DMM, *Proc. 2nd Int. Conf. on Ground Improvement Geosystems* (IS-Tokyo'96), 503-508.
12) Madhav, M. R. and Vitkar, P. P. (1978): Strip footing on weak clay stabilized with granular trench or piles, *Canadian Geotechnical Journal*, **15**, 605-609.
13) Porbaha, A. (1998): State of the art in deep mixing technology, Part I: Basic concepts, *Ground Improvement, Journal of ISSMGE*, **2**(2), 81-92.
14) Porbaha, A., Tanaka, H. and Kobayashi, M. (1998): State of the art in deep mixing technology, Part II: Application areas, *Ground Improvement, Journal of ISSMGE*, **2**(3), 125-139.
15) Porbaha, A., Zen, K. and Kobayashi, M. (1999): Deep mixing technology for liquefaction mitigation, *Journal of Infrastructure Systems*, ASCE, **5**(1), 21-34.
16) Rixner, J. J., Kraemer, S. R. and Smith, A. D. (1986): Prefabricated vertical drains, *Report No. FHWA-RD-86/168*, Federal Highway Administration, Washington D.C.
17) Salençon, J. (1983): Calcul à la rupture et analyse limite, Edit. Presses des Ponts et Chaussées, Paris.
18) Salençon, J. (1990): An introduction to the yield design theory and its applications to soil mechanics, *European Journal of Mechanics*, A/Solids, **9**(5), 477-500.
19) Terashi, M. and Tanaka, H. (1983): Bearing capacity and consolidation of the improved ground by a group of treated columns, *Report of Port and Harbour Research Institute*, **22**(2), 214-233 (in Japanese).

APPENDIX I: DERIVATION OF MAXIMUM RESISTING WORK

The failure mechanism with five blocks (Fig. 5(b)) involves movement of rigid blocks on surfaces (OE), (ON), (EN), (NM) and their symmetric parts where discontinuities of velocity occur. Hence, there is no deformation within the blocks (1), (2), (2′), (3) and (3′) i.e., $d=0$. It follows $\Pi(d)=0$, and from Eq. (3) we have:

$$P(\underline{v}) = \int_{\Sigma} \Pi(n, [v]) d\Sigma = P_1(v) + P_2(v) \tag{24}$$

The discontinuity of v, between blocks i and j, is denoted by $[v]_{ij}$ such that $[v]_{ij} = v_j - v_i$ (The outward unit normal vector n is oriented from block i to block j). According to Salençon (1983), for a Tresca's material with cohesion c, we have:

$$\Pi(n; [v]) = c|[v]| \quad \text{if:} \quad [v] \cdot n = 0 \tag{25}$$

This condition allows only tangential discontinuities of velocity on each part of Σ which can be qualified in this case as sliding surface.

Discontinuities of velocity are determined from the hodograph (Fig. 6) as follows:

(a): on surfaces (OE), (OE′) and similarly on surfaces (ON) and (ON′):

$$|[v]_{12}| = |[v]_{02}| = |[v]_{12'}| = |[v]_{02'}| = U/(2 \sin \alpha) \tag{26a}$$

$$|OE| = |OE'| = |ON| = |ON'| = S/(2 \cos \alpha) \tag{26b}$$

(b): on surfaces (NM) and (N′M′):

$$|[v]_{03}| = |[v]_{03'}| = U/(2 \tan \alpha \cos \delta); \tag{26c}$$

and $$|NM| = |N'M'| = S \tan \alpha / \sin \delta \tag{26d}$$

(c): on surfaces (EN) and (E′N′):

$$|[v]_{23}| = |[v]_{23'}| = U[1 + \tan \delta / \tan \alpha]/2;$$

and $$|EN| = |E'N'| = S \tan \alpha \tag{26e}$$

Starting from Eq. (24) and using Eqs. (25), (26a, 26b, 26c, 26d and 26e), the first contribution of maximum resisting work is:

$$P_1(v) = c_{us} US[\{1 + \eta(K_c - 1)\}/\sin \alpha \cos \alpha + 1/(\sin \delta \cos \delta) + \tan \alpha + \tan \delta] \tag{27}$$

Discontinuities of velocity occur also on the soil-rigid-box contact surfaces by means (NEM), (OEN), (OEE′), (OE′N′), (NE′M′) corresponding to the side $y = -L/2$, and their symmetric parts corresponding to $y = L/2$. Since the hypothesis of low friction contact is assumed on these surfaces, the corresponding terms in $P(v)$ will be calculated by considering a cohesion c'_{us} lower than that of the soft clay, $c'_{us} = kc_{us}$ such that: $0 \leq k < 1$. Calculation of the corresponding term in $P(v)$ is given by:

$$P_2(\underline{v}) = kc_{us} S \frac{B}{L} \left(\frac{1 + \sin \alpha}{2 \cos \alpha} + \frac{\tan \alpha}{\sin \delta} \right) \tag{28}$$

The upper bound value of the bearing capacity is determined from Ineq. (1) by taking into account the Eqs. (8), (12), (27) and (28), as following:

$$\left(\frac{Q^*}{c_{us} S} \right) \leq \frac{1 + \eta(K_c - 1)}{\sin \alpha \cos \alpha} + \tan \alpha + \frac{1}{\sin \delta \cos \delta} + \tan \delta + k \left(\frac{B}{L} \right) \left(\frac{1 + \sin \alpha}{2 \cos \alpha} + \frac{\tan \alpha}{\sin \delta} \right) - \eta(\gamma_c - \gamma_s) \frac{B \tan \alpha}{2 c_{us}}$$

APPENDIX II: INCORPORATION OF GRAVITY FORCES IN THE KINEMATIC APPROACH

Starting from Fig. 5, at the exterior of the blocks $\underline{v_0}$ is equal to zero. The velocity field vectors in the blocks could be determined easily from the hodograph shown in Fig. 6. Considering that: $[v]_{i0} = v_i - v_0 = v_i$, therefore, the vertical components of velocity vectors will be:

—For block (1): $$v_z = -U \tag{29}$$

—For blocks (2) and (2′): $$v_z = -|[v]_{02}| \sin \alpha = -U/2 \tag{30}$$

—For blocks (3) and (3′): $$v_z = |[v]_{03}| \sin \delta = (U \tan \delta)/2 \tan \alpha \tag{31}$$

Then, contribution of gravity forces appearing in Eq. (8) will be determined using Eqs. (29), (30), and (31); and taking into account the weight of each block.

Determination of gravity contribution from Eq. (8), where v_z is constant as given by Eqs. (29), (30), and (31), needs calculation of the volumes of columns in blocks (1) and (2) or (2′) which are denoted $V_c(1)$ and $V_c(2)$ respectively.

The total volume of blocks (1) and (2) is given by:

$$V(1) = V(2) = V = \frac{B^2 L}{4} \tan \alpha \tag{32}$$

For symmetric location of the columns along x axis, as shown in Figs. 5(a) and 5(b), volumes of columns in blocks (1) and (2) are given by the following expressions:

$$V_c(1) = (\eta/3) BL(B/2 + 2b) \tan \alpha \tag{33a}$$

$$V_c(2) = (\eta/3) BL(B - 2b) \tan \alpha \tag{33b}$$

b is the distance between the footing edge and the centreline of the first column (Fig. 5(b)).

In order to derive a simple expression of gravity contribution, it is assumed that $b = B/8$, from which it follows that:

$$V_c(1) = V_c(2) = \eta V \tag{34}$$

In this situation, the unit weight in blocks (1), (2) and (2′) is proportional to the replacement area ratio η. So, by setting:

$$\gamma_m = [(1 - \eta)\gamma_s + \eta \gamma_c] \tag{35}$$

we have:

$$\int_{(1)} \gamma_m d\Omega = \int_{(2)} \gamma_m d\Omega = \int_{(2')} \gamma_m d\Omega = [(1 - \eta)\gamma_s + \eta \gamma_c] \times \frac{B^2 L \tan \alpha}{4} \tag{36}$$

$$\int_{(3')} \gamma_s d\Omega = \int_{(3)} \gamma_s d\Omega = \gamma_s \frac{B^2 L \tan^2 \alpha}{2 \tan \delta} \tag{37}$$

The contribution of gravity forces in all blocks will be calculated using Eqs. (29), (30), (31), (36), and (37), as following:

$$\int_{\Omega_c} \gamma_c v_z d\Omega + \int_{\Omega_s} \gamma_s v_z d\Omega = -U \int_{(1)} \gamma_m d\Omega + 2(-U/2) \times \int_{(2)} \gamma_m d\Omega + 2[(U \tan \delta)/2 \tan \alpha] \times \int_{(3)} \gamma_s d\Omega \quad (38)$$

and finally:

$$\int_{\Omega_c} \gamma_c v_z d\Omega + \int_{\Omega_s} \gamma_s v_z d\Omega = \eta(\gamma_c - \gamma_s) \frac{SBU \tan \alpha}{2}$$

APPENDIX III: LOWER BOUND OF BCF

This approach by inside (referred to as the static approach) of YDT is carried out by the construction of statically admissible (SA) stress fields, i.e. verifying:

- equilibrium equations ($\partial\sigma_{ij}/\partial x_j + \gamma e_z = 0$) where $i, j = x, y, z$,
- stresses boundary conditions given in Eqs. (5), (7a and b);
- continuity of the stress vector expressed by: $T = \sigma \cdot n$

Within the improved scaled models consider the construction of a stress field with four zones (Fig. 5(b)) where stress components are as follows in the (x, y, z) space assumed as a principal:

a) The unimproved soft clay in symmetrical zones (1) and (1′):

$$\sigma_z = \gamma z \quad (39)$$

*Zone (2): the soft clay under the base of the rigid plate:

$$\sigma_z = \gamma z - 4c_{us} \quad (40)$$

- Zone (3): The columns located under the rigid plate:

$$\sigma_z = \gamma z - 2c_{us}(1 + K_c) \quad (41)$$

The continuity of the stress vector between the four zones requires that:

$$\sigma_x = \sigma_y = \gamma z - 4c_{us} \quad (42)$$

In every point of the scaled model, the constructed stress field should comply with Tresca's strength criterion that writes:

$$|\sigma_i - \sigma_j| \leq 2K_c c_{us} \quad (43)$$

where σ_i and σ_j denotes principal stresses and $K_c \geq 1$.

From Eqs. (40), (41), (42) and (43) equilibrium equations and boundary conditions in stresses are verified. Tresca's criterion is not violated. Substituting the vertical stress component (43) in Eq. (9a) because $T_z = \sigma_z e_z$, the best lower bound of BCF is that expressed in the right hand of Ineq. (16). One can note this lower bound of BCF does not depend on gravity when considering equal unit weight for the soft clay and the columns material.